Medical Physics
The International Journal of Medical Physics Research and Practice

Oxygen distribution in tumors: A qualitative analysis and modeling study providing a novel Monte Carlo approach

Jakob H. Lagerlöf, Jon Kindblom, and Peter Bernhardt

Citation: Medical Physics **41**, 094101 (2014); doi: 10.1118/1.4892386
View online: http://dx.doi.org/10.1118/1.4892386
View Table of Contents: http://scitation.aip.org/content/aapm/journal/medphys/41/9?ver=pdfcov
Published by the American Association of Physicists in Medicine

Oxygen distribution in tumors: A qualitative analysis and modeling study providing a novel Monte Carlo approach

Jakob H. Lagerlöf[a)]
Department of Radiation Physics, Göteborg University, Göteborg 41345, Sweden

Jon Kindblom
Department of Oncology, Sahlgrenska University Hospital, Göteborg 41345, Sweden

Peter Bernhardt
Department of Radiation Physics, Göteborg University, Göteborg 41345, Sweden and Department of Nuclear Medicine, Sahlgrenska University Hospital, Göteborg 41345, Sweden

(Received 22 February 2014; revised 8 July 2014; accepted for publication 24 July 2014; published 12 August 2014)

Purpose: To construct a Monte Carlo (MC)-based simulation model for analyzing the dependence of tumor oxygen distribution on different variables related to tumor vasculature [blood velocity, vessel-to-vessel proximity (vessel proximity), and inflowing oxygen partial pressure (pO_2)].
Methods: A voxel-based tissue model containing parallel capillaries with square cross-sections (sides of 10 μm) was constructed. Green's function was used for diffusion calculations and Michaelis-Menten's kinetics to manage oxygen consumption. The model was tuned to approximately reproduce the oxygenational status of a renal carcinoma; the depth oxygenation curves (DOC) were fitted with an analytical expression to facilitate rapid MC simulations of tumor oxygen distribution. DOCs were simulated with three variables at three settings each (blood velocity, vessel proximity, and inflowing pO_2), which resulted in 27 combinations of conditions. To create a model that simulated variable oxygen distributions, the oxygen tension at a specific point was randomly sampled with trilinear interpolation in the dataset from the first simulation. Six correlations between blood velocity, vessel proximity, and inflowing pO_2 were hypothesized. Variable models with correlated parameters were compared to each other and to a nonvariable, DOC-based model to evaluate the differences in simulated oxygen distributions and tumor radiosensitivities for different tumor sizes.
Results: For tumors with radii ranging from 5 to 30 mm, the nonvariable DOC model tended to generate normal or log-normal oxygen distributions, with a cut-off at zero. The pO_2 distributions simulated with the six-variable DOC models were quite different from the distributions generated with the nonvariable DOC model; in the former case the variable models simulated oxygen distributions that were more similar to *in vivo* results found in the literature. For larger tumors, the oxygen distributions became truncated in the lower end, due to anoxia, but smaller tumors showed undisturbed oxygen distributions. The six different models with correlated parameters generated three classes of oxygen distributions. The first was a hypothetical, negative covariance between vessel proximity and pO_2 (VPO-C scenario); the second was a hypothetical positive covariance between vessel proximity and pO_2 (VPO+C scenario); and the third was the hypothesis of no correlation between vessel proximity and pO_2 (UP scenario). The VPO-C scenario produced a distinctly different oxygen distribution than the two other scenarios. The shape of the VPO-C scenario was similar to that of the nonvariable DOC model, and the larger the tumor, the greater the similarity between the two models. For all simulations, the mean oxygen tension decreased and the hypoxic fraction increased with tumor size. The absorbed dose required for definitive tumor control was highest for the VPO+C scenario, followed by the UP and VPO-C scenarios.
Conclusions: A novel MC algorithm was presented which simulated oxygen distributions and radiation response for various biological parameter values. The analysis showed that the VPO-C scenario generated a clearly different oxygen distribution from the VPO+C scenario; the former exhibited a lower hypoxic fraction and higher radiosensitivity. In future studies, this modeling approach might be valuable for qualitative analyses of factors that affect oxygen distribution as well as analyses of specific experimental and clinical situations. [http://dx.doi.org/10.1118/1.4892386]

Key words: Monte Carlo, tumor control probability, dosimetry, modeling, hypoxia, radiotherapy

1. INTRODUCTION

It is well-established that tumor oxygenation influences the outcome of radiation treatment, due to the oxygen enhancement described by Crabtree and Cramer[1] and Mottram[2] around the 1930s. In clinical studies, it has been demonstrated that a low hypoxic fraction in the tumor is associated with improved overall survival after radiotherapy.[3,4] Furthermore, the outcome of radiation treatment can be improved by enhancing the oxygen content of the tumor with hyperbaric techniques and with drugs such as nitroimidazoles, which mimic oxygen enhancement effects after irradiation.[5,6] However, even though meta-analyses of randomized clinical trials that compare the additional effect of the above treatments to ordinary radiation treatment demonstrate improved outcome, the impact of these findings in daily practice has thus far been very limited.[7] The optimal timing and dosage of the respective agents and modalities used in tumor hypoxia modification remain to be established. There is also considerable variability in the hypoxic fraction among patients and in its correlation to the therapeutic outcome.[8,9] With the recent development of noninvasive hypoxia imaging techniques, such as positron emission tomography (PET) and magnetic resonance imaging (MRI), the ability to characterize the distribution of hypoxia in tumors has now improved.[10–12] However, the interpretation of measurements of hypoxia, or more generally, oxygen tension must improve if this information is to be used in treatment planning and for predictions of therapeutic response.

In a previous modeling study, it was shown that neither an average oxygen value nor information about the hypoxic fraction of a tumor was sufficient to estimate the required absorbed dose for a tumor cure. To accurately estimate the required absorbed dose, the entire oxygen distribution must be taken into account.[13] However, simulations of the oxygen distribution are too complex to be efficiently run on common platforms; therefore, simulation models tend to be simplified in different ways. One simplification is to use a relevant mean oxygen content in the blood vessel, often 40 mm Hg. From that, oxygen diffusion into the tumor tissue can be simulated for different blood vessel arrangements.[14] However, it has been shown that, with increasing tumor mass, the mean oxygen tension decreases[15] and the necrotic fraction simultaneously increases.[16] To explore variations in tumor oxygen tension and necrotic fraction with a modeling approach, continuous oxygen consumption along blood vessels must be included.[17] However, that modeling approach lengthened the simulation time (using the CPU of a single up-to-date workstation) beyond that feasible for an effective theoretical investigation in macroscopic tumors with complex interactions between biological parameters. Examples of these parameters are the inflowing oxygen tension, blood velocity, and vessel-to-vessel proximity (vessel proximity). To overcome this limitation, a Monte Carlo-based model was constructed to facilitate the effective theoretical analyses of how variations in biological parameters impact the oxygen distribution and radiosensitivity of different-sized tumors. This facilitation is achieved through rapid sampling of previously generated distributions in order to create correlated parameter scenarios. The use of these scenarios reduces the requirement of simulating every combination individually.

The vascular supply that infiltrates tumors comes from the existing surrounding blood vessels. However, because all growing tumors eventually outgrow the original vascular supply, vascular expansion occurs which leads to chaotic structures, dysfunctional vessels, inadequate lymphatic drainage, increased interstitial pressure, decreased perfusion, hypoxia, and necrosis.[18] Hypoxia is one of the triggers of angiogenesis.[19,20] It is also known to decrease the apoptotic potential of tumor cells[21,22] and can initiate vessel pruning.[23] Due to the complex interactions among these dynamic parameters, the vascular tree associated with a large tumor becomes heterogeneous in architecture and efficiency, and the oxygen distribution becomes unpredictable. However, a known characteristic of the chaotic angiogenesis that occurs in growing tumors is that inflowing oxygen tension varies around the tumor, and the vessel-to-vessel proximity and blood flow vary within the tumor.[16,24,25]

In a previous study, it was observed that oxygen distribution characteristics may provide useful information on the properties of tumor vasculature.[13] The present study aims to expand on our earlier work by investigating the effects that different parameters of vasculature and blood supply have on the oxygen distribution, and in turn, how the oxygen distribution might influence the radiosensitivity of the tumor. In particular, a novel Monte Carlo model is used to estimate oxygen distribution and to analyze different correlations between the oxygen tension of inflowing blood, the vessel proximity, and the blood velocity. Also, the effects of differently correlated parameters on oxygen distribution are compared.

2. METHODS AND MATERIALS

In this study, the renal cell carcinoma (RCC) angiogram [Fig. 1(a)] provides an example of a typical tumor often depicted in simplified models; it is spherical, has vessels leading from the surface toward the center, and has a necrotic core. The image demonstrates variable vessel-to-vessel- proximity (vessel proximity), but does not provide reliable information regarding the efficiency of the vessels because the contrast agent was administered *ex vivo*, under high pressure.[26] Briefly, the surgically removed kidney tumor specimen was perfused with micronized barium sulfate suspensions and fixed in formaldehyde. Then, 1 mm slices were cut, inserted into an envelope of Kodak X-omatic film, and exposed in a mammograph. The exposed film was developed with conventional methods.

Two different models were constructed based on depth oxygenation curves (DOC). The first was a simplified model with no variation in the three biological parameters: blood velocity, vessel proximity, and inflowing oxygen tension. The RCC image, with its necrotic center, was used to qualitatively determine the parameter values; thus, constant values were used which were not necessary valid for the RCC as these cannot be known, but they produced a similar oxygen penetration (judging from the necrotic fraction, which of course in turn depends on the necrosis threshold used). The

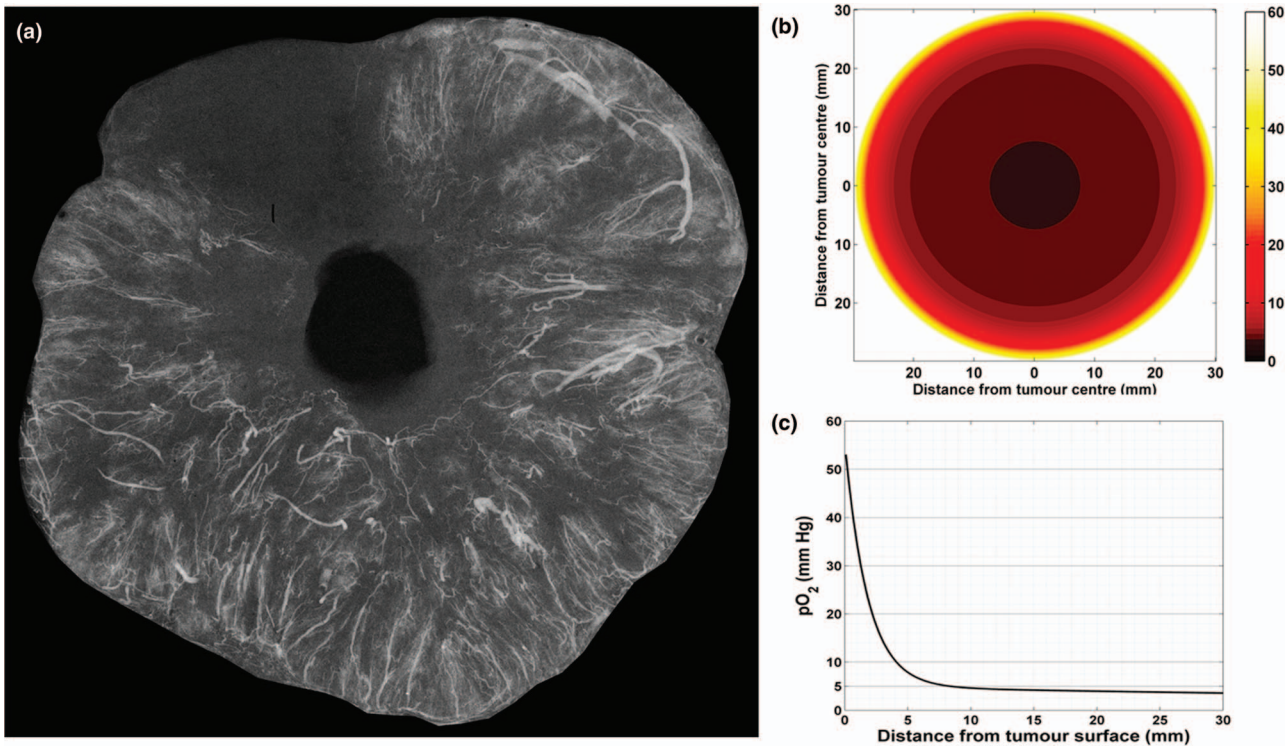

FIG. 1. Simplified tumor oxygenation model. (a) Renal cell carcinoma angiogram; bright, contrast-enhanced vessels demonstrate variability in vessel proximity. (b) Depth oxygenation curve model shows oxygenation in a slice of tumor tissue, radius 30 mm; scale shows color-coded oxygenation levels; black: no oxygen (0 mm Hg); white: 60 mm Hg oxygen. (c) Oxygen tension field that corresponds to the depth of oxygen model shown in (b). The simulation parameters used to generate this data were: constant blood velocity: 2000 μm/s; vessel proximity: 50 μm; inflowing oxygen tension: 80 mm Hg. The pO_2 pressure decreases as a biexponential function ($R^2 = 0.95$) of radial distance to the tumor center.

second model used similar parameter values, but with variability added by random selection of parameter values from a normal distribution.

2.A. Creation of the DOC including tumor geometry

A voxel-based tissue model containing parallel capillaries with square cross sections (sides of 10 μm) and oxygenated blood entering the vessels was constructed. This achieved a DOC that extended 30 mm into the tissue; i.e., the radius of the RCC [Figs. 1(b) and 1(c)]. In this simulation geometry, the capillaries were centered on the nodes of a two-dimensional grid. For the oxygen to diffuse over the entire distance, the grid size (i.e., the vessel proximity) was set to 50 μm—equivalent to a vascular fraction (VF) of 0.08, the blood moved at a velocity of 2000 μm/s,[27,28] and the initial pO_2 was 80 mm Hg. The oxygen tension of the blood was assumed to be homogeneous across the vessel. Diffusion was modeled by repeated convolution of the tissue oxygen tension field matrix with a Gaussian diffusion kernel (Green's function of the diffusion equation)[13] with a time interval of 0.1 s. The maximum oxygen consumption was assumed to be 15 mm Hg/s,[29,30] and the Michaelis-Menten consumption model[13] was used to adjust the oxygen values between each convolution. Tabulated hemoglobin data[31] were used to model equilibrium between the pO_2 of the blood and the hemoglobin saturation.

Due to variations in the distance between individual tissue voxels and nearby vessels, the oxygen tension field across the plane perpendicular to the vessels varied slightly. These variations, however, were small compared to other intratumoral variations, and they rapidly decreased with distance from tumor surface. The values could therefore be averaged across the plane at each depth when the DOC was generated.

2.B. Parameterization of the DOC curves

The oxygen depth curves were used to create a variable tumor oxygenation model (variable DOC model), in which the oxygen level decreased with distance from the tumor surface. The parameter ranges were: intravascular pO_2 (60, 80, 100, mm Hg), blood velocity (1500, 2000, 2500 μm/s), and vessel proximity (30, 40, 50 μm). Twenty-seven parameter combinations were simulated, fitted with biexponential functions (R^2-values were greater than 0.94, typically around 0.99), and stored as separate DOCs. Figure 2 shows some of the data, with tissue oxygen penetration depths shown at different oxygen tension cut-off values.

2.C. The Monte Carlo method, geometry, and sampling

In the variable DOC model, a Monte Carlo approach was used to simulate the oxygen tension at specific points in a spherical tumor inscribed in a cube. A random coordinate was selected within the tumor and the shortest distance to the tumor surface was calculated. An oxygen curve was selected by sampling from three Gaussian distributions: one was the pO_2 centered at 80 with standard deviation (SD) 10 mm Hg, the second was the blood velocity centered at 2000 (SD 250)

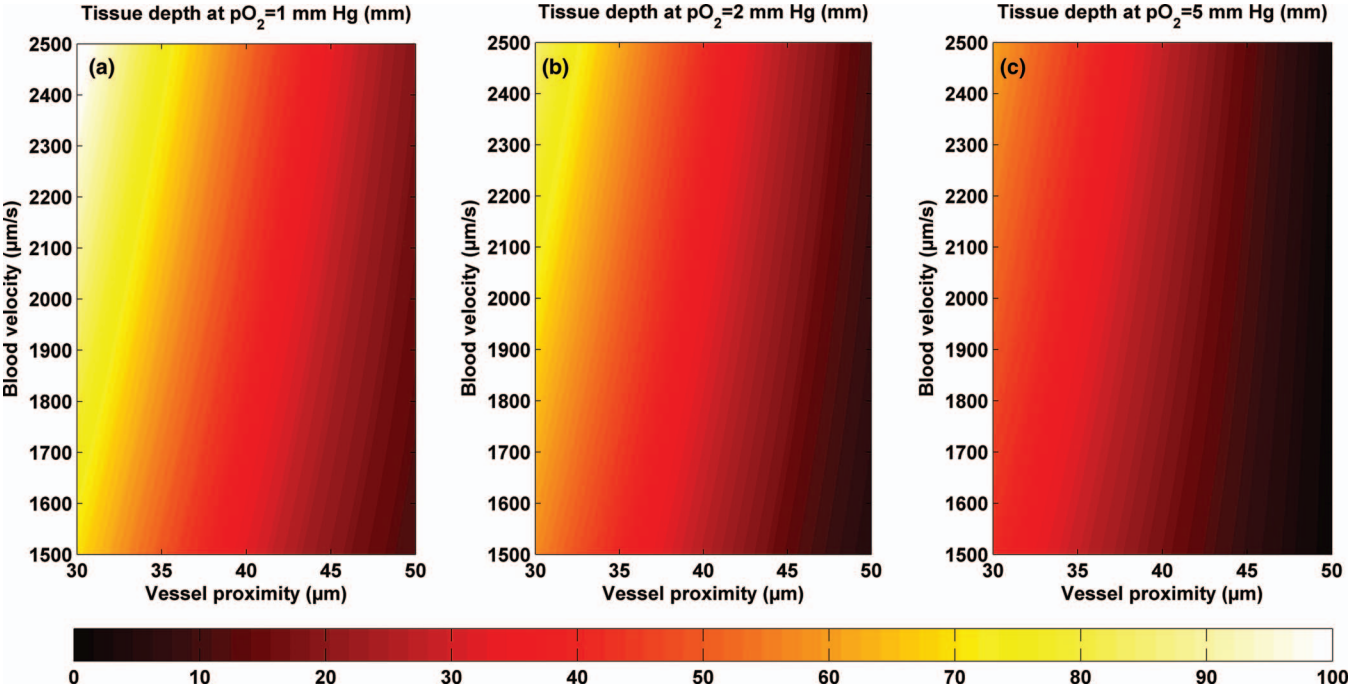

FIG. 2. Depth of oxygen penetration into the tissue for pO_2 cut-off: (a) 1 mm Hg, (b) 2 mm Hg, and (c) 5 mm Hg, versus vessel proximity and blood velocity. The initial vessel pO_2 was 80 mm Hg. The color bar indicates oxygen penetration depths from 0 mm (black) to 100 mm (white).

μm/s, and the third was the vessel proximity centered at 40 (SD 5) μm (corresponding to a VF of 0.125). All distributions were truncated at ± 2 SD. The oxygen level of the tumor coordinate was then determined by interpolation between the oxygen curve functions for the distance between the tumor surface and the coordinate. This procedure was repeated 10 000 times, and the pO_2-values produced a pO_2-distribution representing the tumor.

2.D. The parameter coupling schemes used

The Monte Carlo model was used to compare the oxygen distribution from the nonvariable DOC model (demonstrated in Fig. 1) to six other distributions for tumors with radii of 5, 10, 20, and 30 mm. These distributions were generated with: (1) uncorrelated parameters, (2) corr(pO_2,blood velocity) = 1, (3) corr(pO_2, vessel proximity) = 1, (4) corr(blood velocity, vessel proximity) = 1, (5) corr(pO_2, vessel proximity, blood velocity) = 1, and, finally, (6) corr(pO_2, vessel proximity) = -1. Here, corr represents the correlation coefficient, and corr = 1 indicates that the parameters were selected from the same position in their respective distributions (covariant) in terms of the mean value and standard deviation. Corr = -1 means that the positions in one distribution were mirrored in the other.

2.E. Response to irradiation

The oxygen distributions were converted to oxygen enhancement ratio (OER) distributions according to[32]

$$\mathrm{OER}(pO_2) = 1 + \frac{0.81 \cdot (pO_2)^{0.616}}{1 + 0.324 \cdot (pO_2)^{0.616}}. \quad (1)$$

It was assumed that the cell density was 10^9 cells per cm^3 of tumor tissue, and the radiation sensitivity parameters ($\alpha = 0.02$ and $\beta = 0.002$) were used to produce clinically-relevant absorbed dose levels. The linear quadratic cell survival model was used to calculate the absorbed dose level at a tumor control probability (TCP, the probability of killing every cell in the tumor) of 0.99 (D_{99}-value) for each distribution. This was done according to Eq. (2), where N is the total number of cells in the tumor volume, D is the mean absorbed dose, and OER is the oxygen enhancement ratio,[32]

$$\mathrm{TCP} = \prod_{i=1}^{N} (1 - e^{-\alpha \cdot D \cdot \mathrm{OER}_i - \beta \cdot D^2 \cdot \mathrm{OER}_i^2}). \quad (2)$$

3. RESULTS

The simulations of the oxygen distributions began with the nonvariable DOC model, and used constant values for the inflowing oxygen tension, blood velocity, and vessel proximity. With this model, the induced necrotic fraction was simulated by testing different parameter values and assuming an oxygen tension level of 1 mm Hg for the induction of necrosis (Fig. 1). This nonvariable DOC model generated an oxygen tension that decreased strictly toward the tumor center [Figs. 1(b) and 1(c)]. With the simulations of tumors with radii of 5 and 30 mm, the oxygen tensions tended to have log-normal distributions.

Adopting the MC approach with the variable DOC model, variable values for inflowing oxygen tension, blood velocity, and vessel proximity were included. With this model, most of the oxygen tension distributions sampled [with the exception of corr(pO_2, vessel proximity) = -1] displayed quite

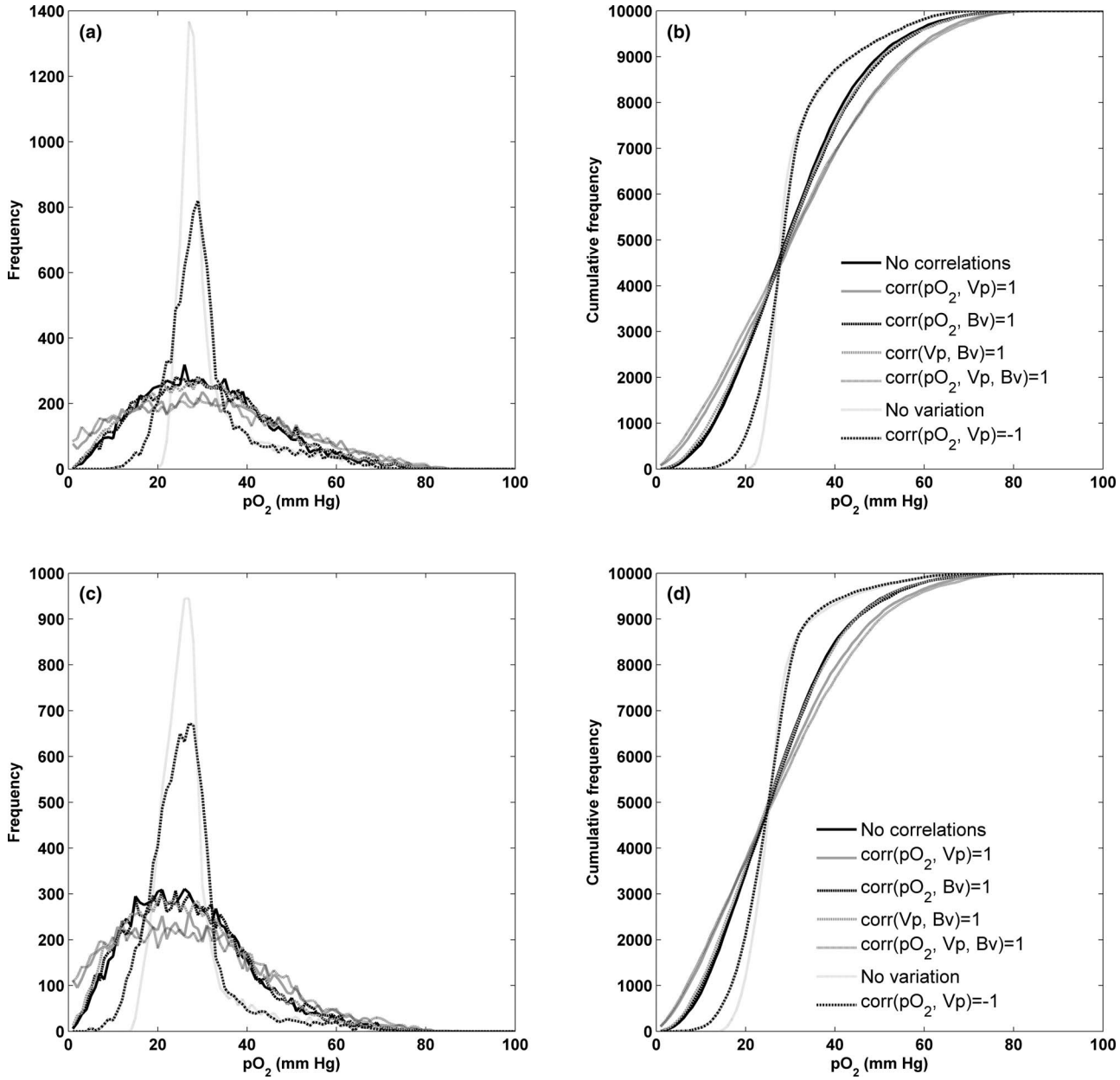

FIG. 3. Hypothetical biological model simulations, including the nonvariable DOC and six variable DOCs, with different correlations between the parameters intravascular pO_2, Vp, and Bv. (a) and (c) Relative volumetric pO_2-distributions for a tumor with a radius of (a) 5 mm or (c) 30 mm; (b) and (d) cumulative pO_2 distributions for a tumor with a radius of (b) 5 mm or (d) 30 mm.

different shapes from the distributions generated with the nonvariable DOC model. The variable DOC model produced distributions similar to the oxygen distributions measured *in vivo*, with normal or log-normal profiles (Fig. 3).[33–35] The shapes of the six distribution-based curves and that of the nonvariation scenario varied and appeared to be more or less divided into three groups:

(1) corr(pO_2, blood velocity) = 1 and corr(vessel proximity, blood velocity) = 1;
(2) corr(pO_2, vessel proximity) = 1 and corr(pO_2, vessel proximity, blood velocity) = 1; and
(3) corr(pO_2, vessel proximity) = −1 and "No variation."

These groupings are most clearly visible in the cumulative pO2 distributions shown in Figs. 3(b) and 3(d).

The following three correlations were further studied and will henceforth be referred to in terms of hypothetical biological models, to be described in Sec. 4. These are defined as: the hypothetical uncorrelated parameter (UP) scenario; the hypothetical vessel proximity oxygen positive covariance (VPO+C) scenario, with the parameters corr(pO_2, vessel proximity) = 1; and the hypothetical vessel proximity oxygen negative covariance (VPO-C) scenario, with the parameters corr(pO_2, vessel proximity) = −1. The "No variation" (DOC) model was included for comparison.

Figure 4 shows the spatial distributions of oxygen pressure from simulations with the nonvariable DOC model

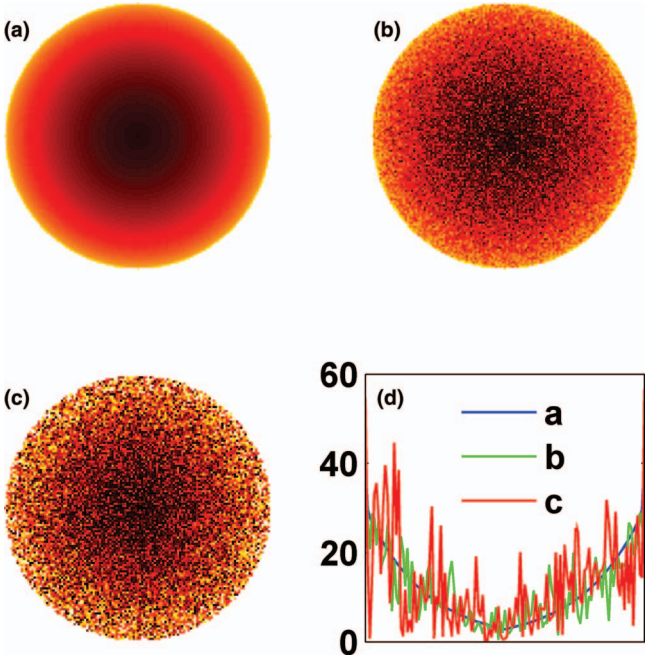

FIG. 4. Simulated spatial oxygen distributions in the central plane of a tumor with radius 30 mm, displayed in a 128 × 128 matrix. Mean inflowing oxygen tension was 80 mm Hg, vessel proximity was 40 μm, and blood velocity was 2000 μm/s. (a) The nonvariable DOC model; (b) the VPO-C model with a surface pO_2 SD = 10 mm Hg, a vessel proximity SD = 5 μm, and a blood velocity SD = 250 μm/s; (c) the VPO+C model with the same SDs; (d) profile lines showing the oxygen tension levels along the tumor diameter for distributions (a)–(c).

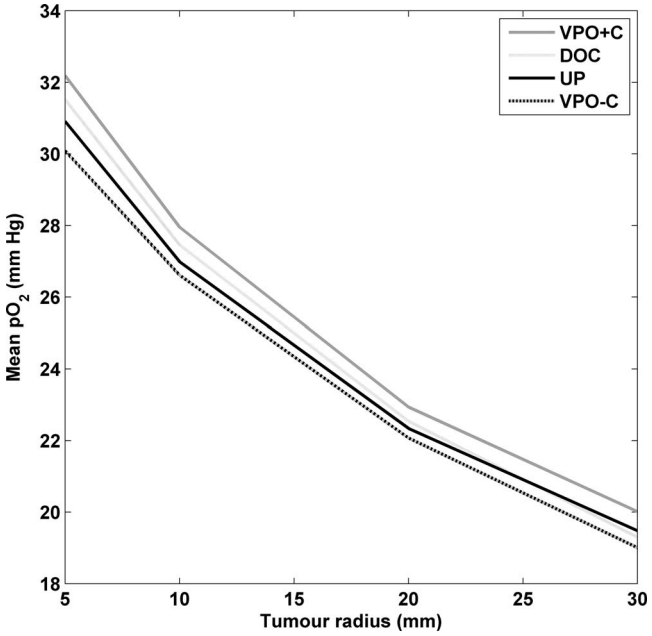

FIG. 5. Mean pO_2 for the nonvariable DOC model and three variable DOC models, with different correlation scenarios. The mean tumor pO_2 for each scenario is shown for tumors with radii of 5, 10, 20, and 30 mm and interpolated for intermediate sizes.

[Fig. 4(a)] and two of the Monte Carlo scenarios: the VPO-C [Fig. 4(b)] and the VPO+C [Fig. 4(c)]. In addition, the respective profile lines [Fig. 4(d)] showed that the VPO-C scenario produced smaller variations in oxygen tension than the VPO+C scenario.

Figure 5 shows that the mean oxygen tension for all scenarios steadily decreased with increasing tumor size. The lowest mean oxygen tension was observed with the VPO-C scenario, and the highest was observed with the VPO+C scenario.

Figure 6 shows tumor hypoxic fractions for all scenarios. The VPO+C scenario showed the largest hypoxic fractions, and the VPO-C showed the smallest fractions. The results indicated that the degree of hypoxic fraction was strongly dependent on the oxygen tension threshold.

Figure 7 shows the tumor radiation sensitivity, in terms of D_{99}-values, for each simulated oxygen distribution as a function of tumor radius. The highest D_{99} values were observed for the VPO+C scenario and the lowest values were observed for the VPO-C scenario.

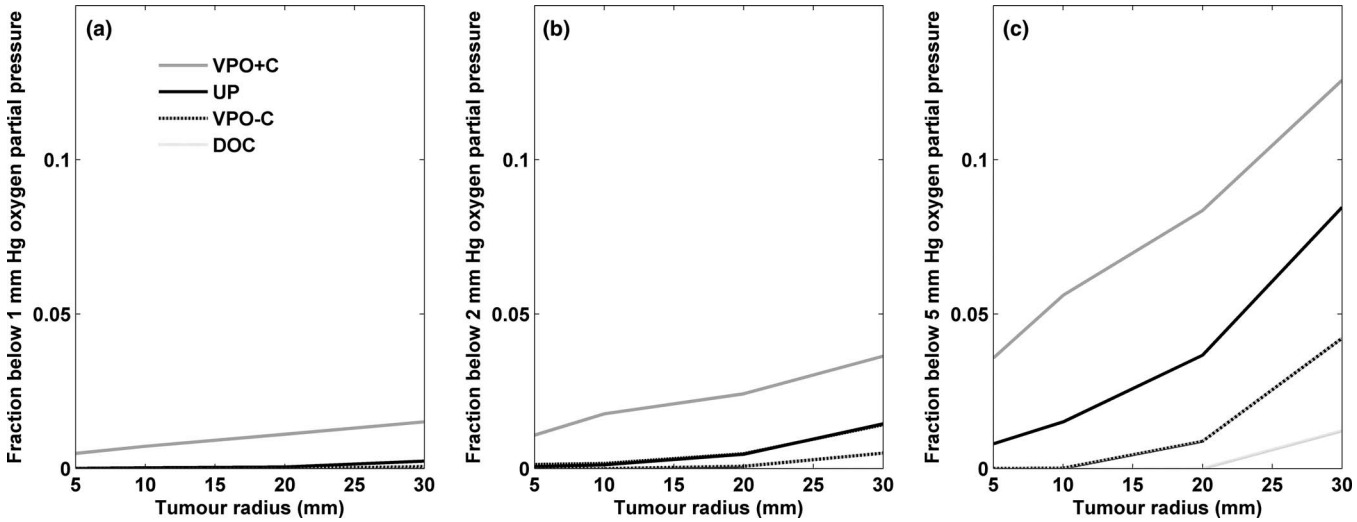

FIG. 6. Fractions of tumor hypoxia. The hypoxic fractions are shown for different oxygen tension thresholds, defined as (a) 1 mm Hg, (b) 2 mm Hg, and (c) 5 mm Hg. Hypoxic fractions are shown for different sized tumors with radii of 5–30 mm, simulated with models that represent different correlation scenarios.

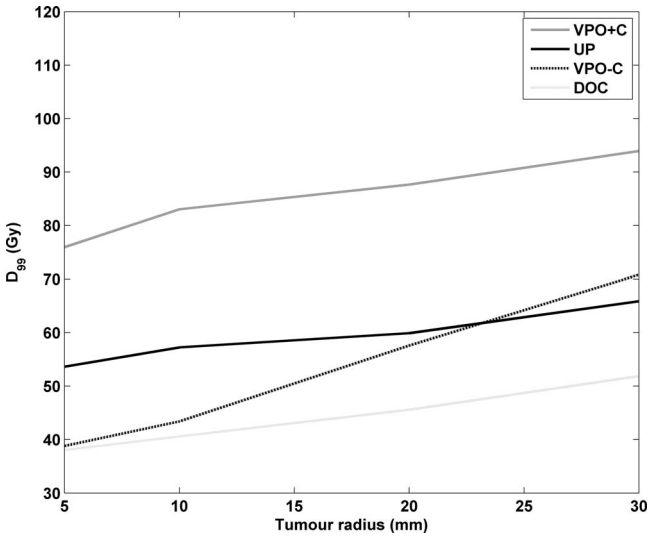

FIG. 7. D_{99} for tumors of different sizes. Different correlation scenarios were used to simulate absorbed dose requirements.

4. DISCUSSION

A new Monte Carlo model for analyzing the impact of relevant biological parameters on tumor oxygen distributions was constructed. Our results demonstrated that the model was robust and, within a reasonable time (about a minute on a 2.5 GHz Intel Core i5-2520M computer running 64-bit Matlab), generated results for tumors of different sizes. The performance of a numerical model such as this is dependent on the number of calculations required, which is determined by the time resolution in the simulations. A higher resolution would lengthen the calculation time, and it would also require higher spatial resolution due to the limited rate of diffusion; thus, a smaller tumor size would be needed to complete the simulation in the same time frame. Moreover, the use of short time steps would require more knowledge about the dynamics of the modeled processes. In essence, there is a modeling accuracy-performance trade-off that one must take into account, but there is also a limit to how much accuracy is required. This study focused on qualitative analyses. The assumed distributions of the model variables were hypothetical estimates that are likely to differ in clinical and preclinical situations. The assumed normal distribution of vessel proximity could have been exchanged with a normally distributed vascular fraction, which would have given a slightly different result because those properties are not linearly related.

The simulation was started assuming constant input parameters. This generated a DOC that strictly decreased to the tumor center with spherical symmetry. This type of oxygen distribution might be generated in tumors with perfectly balanced angiogenesis; i.e., it would lack variation in all parameter values. However, this perfectly symmetrical oxygen distribution is seldom observed in preclinical and clinical studies; instead a broader, somewhat skewed, bell shaped distribution is commonly observed, such as those simulated with dynamic parameter values.[33–35] The grouping of the results from the correlation study implied that it was not particularly important whether the blood velocity was correlated to the other parameters. In contrast, the models produced different results when pO_2 and vessel proximity were correlated, compared to the results when they were not correlated. When vessel proximity and pO_2 had a positive covariance (VPO+C scenario), they tended to work together, thereby increasing the variation and broadening the distribution. When these parameters had a negative covariance (VPO-C, scenario), they tended to oppose each other, resulting in a more homogeneous distribution.

The latter combination, VPO-C, may have superior biological relevance compared to the other scenarios. Two biological phenomena might be represented by VPO-C, hypoxia-driven angiogenesis,[19] and self-regulation of vessel proximity.[20] Hypoxia-driven angiogenesis begins with reduced oxygen pressure, which suppresses the expression of cellular oxygen sensors, prolyl-hydroxylase domain proteins (PDH 1-3). The reduction in PDHs prevents the ubiquitination and degradation of hypoxia inducible factors (HIFs). Thus, active HIFs promote the transcription of hypoxia-related genes [such as vascular epithelial growth factor, VEGF (Ref. 19] which promote angiogenesis. These proangiogenic factors (such as VEGF) stimulate angiogenesis, which results in an increase in vessel proximity. Alternatively, the self-regulation of the vessel proximity phenomenon is based on the fact that each vessel is surrounded by a viable tissue volume that depends on the penetration depth of oxygen and the metabolic activity of the cells. A decrease in pO_2 in the blood will lead to decreased tissue oxygenation, followed by the induction of apoptosis in the distant cells. The induction of apoptosis will reduce the number of cells between blood vessels, and therefore, the vessel proximity increases in oxygen-deficient areas.[20]

All of these variable scenarios had noticeable log-normal distributions, similar to what was previously encountered.[13,33] However, judging from the tumor hypoxic fraction or necrosis, the nonvariable scenario appeared to be the most unlikely to represent biology, because large tumors often harbor large volumes of poorly oxygenated tissue.

In this hypothetical model with positive correlation between pO_2 and vessel proximity (VPO+C), the hypothesis was fairly speculative due to the limited data that are available to support this complex scenario. However, it is known that hypoxia decreases the apoptotic potential, and thus, tumor cells distant from the vessels will not undergo apoptosis, as in the VPO-C scenario.[35–37] When the oxygen tension is sufficiently high in nearby vessels, the tumor cells can proliferate, which would decrease the vessel proximity. In addition, this could also increase the mechanical pressure on the vessels, which might cause acute hypoxia.[23] Further decreases in oxygen tension would force the vascular endothelial cells to undergo apoptosis, and this would result in a further reduction in vessel proximity. Interestingly, the oxygen distributions showed the greatest difference between the VPO-C and the VPO+C models; this information might be useful for future characterizations of tumors with PET and MRI methods that enable visualization of tumor oxygen distributions. For example, tumors that represent the VPO+C scenario would be expected to have higher vessel proximity variation within the tumor tissue, as well as a more flattened

oxygen distribution, compared to tumors that represent the VPO-C scenario. The more peak-shaped VPO-C oxygen distribution might therefore be distinguishable by PET or MRI methods, given the potential for PET- or MRI-characterization of tumors as (VPO-C) radiosensitive. This might be useful data for radiotreatment planning. However, flattened distributions, as produced by the VPO+C scenario (radioresistant) and UP scenario (radiosensitive), will be more challenging to distinguish by PET and MRI methods, due to the limited resolution of the camera systems. Also, flattened oxygen distributions described previously[34,35] might be considered a combination of the biological phenomena discussed above. The possibility that PET and MRI methods can distinguish the different scenarios is of high interest for further studies.

In our simulations, the oxygen tension had a simple linear correlation to vessel proximity. However, in reality, this correlation would probably not be linear. In this study, our purpose was to qualitatively compare two extreme opposite views of dynamic vessel arrangements during tumor growth. Our results showed a clear difference between the scenarios, which highlighted the need for applying more detailed, nonlinear correlation models to the investigation of these phenomena. Recently, Secomb *et al.*[23] performed a theoretical dynamics study on the complexities of building vessel structures during angiogenic conditions. Their approach provided important information about the angiogenic process at a local level of resolution. Combining local tissue modeling with our more global approach is highly important for extending the modeling of oxygen tension to different sized tumors and for analyzing in detail the different biological theories of vessel formation.

Oxygen levels within tumors were shown to be an important factor in the therapeutic outcome of radiation treatments.[4,5,38] Therefore, the impact of radiation on the different correlation scenarios described above was tested. The analysis was performed by applying a single radiation exposure and estimating the absorbed dose required for a tumor control probability of 0.99. The rationale for applying a single exposure model was to focus on the radiation effect by excluding additional parameters in the modeling approach. For example, growth and cell kill dynamics would be required for an accurate estimation of fractionated radiation treatment protocols, but that would introduce new uncertainties in the estimates. Nevertheless, that type of modeling approach will be of interest in future modeling studies of reoxygenation in fractionated treatment protocols. The oxygen enhancement ratio used in this single exposure model was based on adapting the values from Kirkpatrick *et al.*[32] to the linear quadratic model. This modeling approach has shown good agreement with experimental studies.[39] The results from the present D_{99} study clearly showed that, in general, a smaller tumor requires a lower absorbed dose. That was expected, because smaller tumors have fewer cells to kill. Improving tumor oxygenation should decrease the number of hypoxic cells, and therefore, lower the D_{99}. In general this is true, but in some situations, an increase in oxygen may generate an increased number of poorly oxygenated cells in previously anoxic areas; this would lead to the opposite net effect on the required absorbed dose. The consequences of this effect depend on where the "necrosis level" of oxygen tension is set, because this determines the necrotic (no need to kill) and hypoxic (hard to kill) fractions. The present study was not designed to address which oxygen tension setting would be appropriate. Only completely anoxic cells were excluded from the absorbed dose calculations, i.e., a necrotic threshold of 0 mm Hg was used which suppressed this effect.

This study demonstrated that the hypoxic and necrotic fractions increased with tumor size, similar to previous experimental observations.[16,40] These results indicated that the hypoxic and necrotic fractions were smaller when the pO_2 counteracted vessel proximity; this finding suggested that it would be beneficial for tumors to be able to regulate the amount of angiogenesis that occurred in oxygen-depleted situations. With a low necrotic fraction, more cells would be able to proliferate. Consequently, one may conjecture that a tumor with a well-tuned sensitivity for inducing angiogenesis at a rate proportional to the inverse oxygen tension would have a higher proliferation rate, at least if it has a clinically observable size, with radius from 5 to 25 mm. Ultimately, the consequence of fine-tuned angiogenesis would be a minimization of parameter variations. Our study showed that the fastest tumor growth rate could be achieved in a scenario with no variation in the parameter values.

5. CONCLUSION

A novel Monte Carlo algorithm that simulated tumor oxygen distributions and radiation response was presented. This model was based on various hypothetical biologically relevant parameter values. The analysis showed that a self-regulated, hypoxia-driven angiogenesis (VPO-C) scenario generated a clearly different oxygen distribution from other hypothetical scenarios. The VPO-C scenario maintained a low tumor necrotic fraction, closest to that observed in the nonvariable scenario. In future studies, this modeling approach might be valuable for general analyses of factors that affect the oxygen distribution, and for analyses of specific experimental and clinical situations.

ACKNOWLEDGMENTS

This work was supported by grants from the Swedish National Cancer Society, the Swedish radiation safety authority, and the King Gustav V Jubilee Clinic Cancer Research Foundation.

The authors are most grateful to Ragnar Hultborn at the department of oncology, Sahlgrenska University Hospital, Göteborg, Sweden, for providing the angiogram of a human renal cell carcinoma. The authors have no conflict of interest.

[a]Author to whom correspondence should be addressed. Electronic mail: Jakob@radfys.gu.se; Telephone: +46 31 342 88 78.

[1]H. G. Crabtree and W. Cramer, "The action of radium on cancer cells. II. Factors determining the susceptibility of cancer cells to radium," Proc. R. Soc. Lond. B **113**, 238–250 (1933).

[2]J. C. Mottram, M. B. Lond, and D. P. H. Cantab, "Experiments on the radiation of tumours," Br. Med. J. **1**, 275–277 (1927).
[3]M. Nordsmark, S. M. Bentzen, V. Rudat, D. Brizel, E. Lartigau, P. Stadler, A. Becker, M. Adam, M. Molls, J. Dunst, D. J. Terris, and J. Overgaard, "Prognostic value of tumor oxygenation in 397 head and neck tumors after primary radiation therapy. An international multi-center study," Radiother. Oncol. **77**, 18–24 (2005).
[4]M. Höckel, K. Schlenger, B. Aral, M. Mitze, U. Schaffer, and P. Vaupel, "Association between tumor hypoxia and malignant progression in advanced cancer of the uterine cervix," Cancer Res. **56**, 4509–4515 (1996).
[5]M. Saunders and S. Dische, "Clinical results of hypoxic cell radiosensitisation from hyperbaric oxygen to accelerated radiotherapy, carbogen and nicotinamide," Br. J. Cancer Suppl. **27**, S271–S278 (1996).
[6]M. R. Horsman and D. W. Siemann, "Pathophysiologic effects of vascular-targeting agents and the implications for combination with conventional therapies," Cancer Res. **66**, 11520–11539 (2006).
[7]J. Overgaard, "Hypoxic radiosensitization: Adored and ignored," J. Clin. Oncol. **25**, 4066–4074 (2007).
[8]P. Vaupel, K. Schlenger, C. Knoop, and M. Hockel, "Oxygenation of human tumors: Evaluation of tissue oxygen distribution in breast cancers by computerized O2 tension measurements," Cancer Res. **51**, 3316–3322 (1991).
[9]M. Nordsmark, J. Loncaster, C. Aquino-Parsons, S. C. Chou, V. Gebski, C. West, J. C. Lindegaard, H. Havsteen, S. E. Davidson, R. Hunter, J. A. Raleigh, and J. Overgaard, "The prognostic value of pimonidazole and tumour pO2 in human cervix carcinomas after radiation therapy: A prospective international multi-center study," Radiother. Oncol. **80**, 123–131 (2006).
[10]H. Kurihara, N. Honda, Y. Kono, and Y. Arai, "Adiolabelled agents for PET imaging of tumor hypoxia," Curr. Med. Chem. **19**, 3282–3289 (2012).
[11]J. M. Price, S. P. Robinson, and D. M. Koh, "Imaging hypoxia in tumours with advanced MRI," J. Nucl. Med. Mol. Imaging **57**, 257–270 (2013).
[12]V. R. Bollineni, E. M. Wiegman, J. Pruim, H. J. Groen, and J. A. Langendijk, "Hypoxia imaging using positron emission tomography in non-small cell lung cancer: Implications for radiotherapy," Cancer Treatment Rev. **38**, 1027–1032 (2012).
[13]J. H. Lagerlof, J. Kindblom, E. Cortez, K. Pietras, and P. Bernhardt, "Image-based 3D modeling study of the influence of vessel density and blood hemoglobin concentration on tumor oxygenation and response to irradiation," Med. Phys. **40**, 024101 (7pp.) (2013).
[14]A. Dasu, I. Toma-Dasu, and M. Karlsson, "Theoretical simulation of tumour oxygenation and results from acute and chronichypoxia," Phys. Med. Biol **48**, 2829–2842 (2003).
[15]P. Wachsberger, R. Burd, and A. P. Dicker "Tumor response to ionizing radiation combined with antiangiogenesis or vascular targeting agents: Exploring mechanisms of interaction," Clin. Cancer Res. **9**, 1957–1971 (2003).
[16]A. A. Khalil, M. R. Horsman, and J. Overgaard "The importance of determining necrotic fraction when studying the effect of tumour volume on tissue oxygenation," Acta Oncol. **34**, 297–300 (1995).
[17]J. H. Lagerlof, J. Kindblom, and P. Bernhardt, "The impact of including spatially longitudinal heterogeneities of vessel oxygen content and vascular fraction in 3D tumour oxygenation models on predicted radiation sensitivity," Med. Phys. **41**, 044101 (8pp.) (2014).
[18]P. Carmeliet and R. K. Jain, "Angiogenesis in cancer and other diseases," Nature (London) **407**, 249–257 (2000).
[19]S. Goel, D. G. Duda, L. Xu, L. L. Munn, Y. Boucher, D. Fukumura, and R. K. Jain "Normalization of the vasculature for treatment of cancer and other diseases," Physiol. Rev. **91**, 1071–1121 (2011).
[20]L. Hlatky, P. Hahnfeldt, and J. Folkman, "Clinical application of antiangiogenic therapy: Microvessel density, what it does and doesn't tell us," J. Natl. Cancer Inst. **94**, 883–893 (2002).
[21]J. T. Erler, C. J. Cawthorne, K. J. Williams, M. Koritzinsky, B. G. Wouters, C. Wilson, C. Miller, C. Demonacos, I. J. Stratford, and C. Dive, "Hypoxia-mediated down-regulation of Bid and Bax in tumors occurs via hypoxia-inducible factor 1-dependent and -independent mechanisms and contributes to drug resistance," Mol. Cell. Biol. **24**, 2875–2889 (2004).
[22]E. C. Finger and A. J. Giaccia, "Hypoxia, inflammation, and the tumor microenvironment in metastatic disease," Cancer Metastasis. Rev. **29**, 285–293 (2010).
[23]T. W. Secomb, J. P. Alberding, R. Hsu, M. W. Dewhirst, and A. R. Pries, "Angiogenesis: An adaptive dynamic biological patterning problem," PLoS Comput. Biol. **9**, e1002983 (2013).
[24]M. W. Dewhirst, C. Y. Tso, R. Oliver, C. S. Gustafson, T. W. Secomb, and J. F. Gross, "Morphologic and hemodynamic comparison of tumor and healing normal tissue," Int. J. Radiat. Oncol., Biol., Phys. **17**, 91–99 (1989).
[25]J. L. Alcázar, M. J. Galán, M. Jurado, and G. López-García, "Intratumoral blood flow analysis in endometrial carcinoma: Correlation with tumor characteristics and risk for recurrence," Gynecol. Oncol. **84**, 258–262 (2002).
[26]E. Tveit, L. Weiss, S. Lundstam, and R. Hultborn, "Perfusion characteristics and norepinephrine reactivity of human renal carcinoma," Cancer Res. **47**, 4709–4713 (1987).
[27]K. P. Ivanov, M. K. Kalinina, and Yu. I. Levkovich, "Blood flow velocity in capillaries of brain and muscles and its physiological significance," Microvas. Res. **22**, 143–155 (1981).
[28]B. Schrope, V. L. Newhouse, and V. Uhlendorf, "Simulated capillary blood flow measurement using a nonlinear ultrasonic contrast agent," Ultrason. Imaging **14**, 134–158 (1992).
[29]T. W. Secomb, R. Hsu, M. W. Dewhirst, B. Klitzman, and J. F. Gross, "Analysis of oxygen transport to tumor tissue by microvascular networks," Int. J. Radiat. Oncol., Biol., Phys. **25**, 481–489 (1993).
[30]B. W. Pogue, J. O'Hara, C. M. Wilmot, K. D. Paulsen, and H. M. Swartz, "Estimation of oxygen distribution in RIF-1 tumours by diffusion model-based interpretation of pimonidazole hypoxia and Eppendorf measurements," Radiat. Res. **155**, 15–25 (2001).
[31]J. W. Severinghaus, "Simple, accurate equations for human blood O2 dissociation computations," Appl. Physiol. Respir. Environ. Exerc. Physiol. **46**, 599–602 (1979).
[32]J. P. Kirkpatrick, L. I. Cardenas-Navia, and M. W. Dewhirst, "Predicting the effect of temporal variations in PO2 on tumor radiosensitivity," Int. J. Radiat. Oncol., Biol., Phys. **59**, 822–833 (2004).
[33]J. H. Lagerlof, J. Kindblom, and P. Bernhardt, "3D modeling of effects of increased oxygenation and activity concentration in tumors treated with radionuclides and antiangiogenic drugs," Med. Phys. **38**, 4888–4893 (2011).
[34]F. Hyodo, R. M. Davis, E. Hyodo, S. Matsumoto, M. C. Krishna, and J. B. Mitchell, "The relationship between tissue oxygenation and redox status using magnetic resonance imaging," Intl. J. Oncol. **41**, 2103–2108 (2012).
[35]T. G. Graeber, C. Osmanian, T. Jacks, D. E. Housman, C. J. Koch, S. W. Lowe, and A. J. Giaccia, "Hypoxia-mediated selection of cells with diminished apoptotic potential in solid tumours," Nature (London) **379**, 88–91 (1996).
[36]M. Kilic, H. Kasperczyk, S. Fulda, and K. M. Debatin, "Role of hypoxia inducible factor-1 alpha in modulation of apoptosis resistance," Oncogene **26**, 2027–2038 (2007).
[37]A. E. Greijer and E. van der Wall, "The role of hypoxia inducible factor 1 (HIF-1) in hypoxia induced apoptosis," J. Clin. Pathol. **57**, 1009–1014 (2004).
[38]H. Harada, "How can we overcome tumor hypoxia in radiation therapy?," J. Radiat. Res. **52**, 545–556 (2011).
[39]D. J. Carlson, R. D. Stewart, and V. A. Semenenko, "Effects of oxygen on intrinsic radiation sensitivity: A test of the relationship between aerobic and hypoxic linear-quadratic (LQ) model parameters," Med. Phys. **33**, 3105–3115 (2006).
[40]C. G. Milross, S. L. Tucker, K. A. Mason, N. R. Hunter, L. J. Peters, and L. Milas, "The effect of tumor size on necrosis and polarographically measured pO_2," Acta Oncol. **36**, 183–189 (1997).